Journal of Applied Geophysics 97 (2013) 97–106

Contents lists available at ScienceDirect

Journal of Applied Geophysics

journal homepage: www.elsevier.com/locate/jappgeo

# Imaging weak zones in the foundation using frequency domain attenuation tomography

V.R. Balasubramaniam [a,b,*], P.C. Jha [a], E. Chandrasekhar [b], B. Butchi Babu [a], Y.V. Sivaram [a], N. Sandeep [a]

[a] National Institute of Rock Mechanics, Champion Reefs, P.O., Kolar Gold Fields 563117, India
[b] Department of Earth Sciences, Indian Institute of Technology Bombay, Powai, Mumbai 400076, India

ARTICLE INFO

*Article history:*
Received 27 March 2013
Accepted 3 June 2013
Available online 13 June 2013

*Keywords:*
Foundation
Step Frequency GPR
Frequency domain attenuation tomography
Weak zone

ABSTRACT

Cross-hole imaging method using Time Domain (TD) and Frequency Domain (FD) parts of cross-hole radar tomography data acquired using Step Frequency Ground Penetrating Radar (SFGPR) was implemented. This method was adopted for imaging foundation of a dam to check if the foundation was free of geological weak zones. The dam site is characterised by massive and jointed-phyllites associated with major and minor shears. The cross-hole radar tomography data was acquired in the frequency bandwidth of 250 MHz, from the deepest level gallery up to a depth of 40 m in the foundation. In TD, first arrival time and amplitudes of radio waves were inverted using Simultaneous Iterative Reconstruction Technique (SIRT) resulting in velocity and attenuation tomograms. The tomograms showed nearly uniform velocity or attenuation structure in the respective tomographic plane. Subsequently, cross-hole radar tomography data was analysed in FD for a variation of spectrum-amplitude at different frequencies. Amplitudes picked at each single frequency were then inverted using SIRT for obtaining frequency domain attenuation tomogram (FDAT). The FDAT clearly showed presence of anomalous high attenuation zones in the depth range of 23–33 m of the tomographic plane. The anomalous zones in the attenuation tomogram are weak zones in the foundation. To validate the above observations, cross-hole seismic tomography was also done in the same boreholes. Cross-hole seismic tomography results showed low velocity (p-wave) zones around the same location corresponding to the high attenuation zone in FDAT, bringing the dormant weak zone to light. This enabled fine-tuning of the reinforcement design and strengthening the weak zone. This paper discusses the cross-hole radar tomography imaging method, the results of its application in imaging weak zones in the foundation and the comparison of cross-hole radar tomography results (in TD and FD) with the cross-hole seismic tomography results.


## 1. Introduction

Cross-hole tomography is one of the high resolution imaging techniques adopted for imaging subsurface targets, when the depth and size of target are beyond the resolving power of near surface geophysical techniques. Different near surface geophysical techniques can be found in literature (Butler, 2007; Dahlin, 1996; Everett, 2012; Hinze, 1990; Pellerin, 2002; Steeples, 2001; Woolery, 2002; Yule et al., 1998). Cross-hole tomography is preferred as it is a viable alternative geophysical imaging technique, where surface survey is not possible due to limited area of interest for investigation. There are different cross-hole geophysical techniques based on seismic, electrical and electromagnetic methods (Angioni et al., 2003; Deceuster et al., 2006; Deidda and Ranieri, 2005; Jung and Kim, 1999; Saito et al., 1990; Wadhwa et al., 2009). Among such techniques, cross-hole radar tomography is generally preferred owing to its high resolving power enabled by the use of very high frequency ranges (microwaves), for the given probing depth and non-destructive imaging capability (Davis and Annan, 1989; Jha et al., 2002; Valle et al., 1999).

Cross-hole radar tomography has been applied for a variety of objectives for imaging targets of size ranging from few millimetres to few metres using various techniques based on data acquisition, processing and analysis for imaging targets (Holliger et al., 2001; Klotzsche et al., 2010; Valle et al., 1999; Vasco et al., 1997; Wänstedt et al., 2000). Each of those studies has been successful in imaging subsurface targets to a different degree of resolution and accuracy and majority of the cross-hole radar studies involve treating the tomography data in Time Domain (TD). In TD, time and amplitude of radar waves in the media are generally used for imaging the rockmass and other targets. The cross-hole radar tomography images obtained by inversion of time and amplitude are useful in quickly reconstructing the image of the subsurface medium in terms of its velocity and attenuation structures. For most geological materials, the dielectric permittivity varies between 3–40 F/m. Presence of water or air influences the dielectric permittivity of the rock mass and thereby the travel time of propagation in the geological material (Nuzzo et al., 2008). However, in geological materials

* Corresponding author at: National Institute of Rock Mechanics, Champion Reefs, P.O., Kolar Gold Fields, 563117, India. Tel.: +91 8153 275009; fax: +91 8153 275002.
*E-mail address:* vrbala.nirm@gmail.com (V.R. Balasubramaniam).

0926-9851/$ – see front matter © 2013 Elsevier B.V. All rights reserved.
http://dx.doi.org/10.1016/j.jappgeo.2013.06.003

the radar wave velocity does not generally vary significantly as to enable deciphering subtle variation in rock mass conditions. Hence, poor velocity contrast reduces resolving power. The resolving power of such TD technique is also influenced by size of the target, separation of boreholes, ray path coverage, and sensitivity of EM waves to the change in electrical properties between the target and the host medium. For a medium characterised by poor dielectric permittivity contrast, variation in conductivity of the medium can be a useful alternative as conductivity strongly influences the amplitude along the path of propagation of radio waves (Hinz and Bradford, 2010; Holliger et al., 2001; Zhou and Fullagar, 2001). Higher conductivity is well known to impart higher attenuation of radio wave amplitudes. However, amplitude variations are not always commensurate with the conductivity as amplitude is also influenced by geometric spreading, multiple scattering or diffraction, antenna radiation pattern and transmission (Quan and Harris, 1997). Therefore, it is often difficult to obtain reliable attenuation estimates always from the amplitude decay method. Moreover, in order to resolve subsurface features based on attenuation structure, a sufficient contrast in conductivity is essential.

In FD, studies based on transmission and measurement of monofrequency (Cote et al., 1995), estimating attenuation (Quan and Harris, 1997), studying pulse broadening by centroid frequency down shift (Liu et al., 1998), material–signal interaction (Grandjean et al., 2000), mapping conductive zones in the subsurface (Zhou et al., 2001) and imaging media heterogeneity using phase and amplitude inversion (Ellefsen et al., 2011) have demonstrated the effectiveness of the FD approach in tomographic imaging. However, since most of such studies have been conducted using impulse GPR (IGPR), they have predominantly relied on data transformed from TD. Analysing target responses as acquired in raw and pre-transformed data is one of the possibilities for better resolution of the subsurface targets, which is made possible in frequency domain radars. Moreover, frequency of signal holds some additional clues for understanding the nature of the medium or target under study (Annan and Cosway, 1992; Bradford, 2007; Reynolds, 2000). FD processing and analysis of data can help bring out such important information and help improve the resolution of the target. Hence, as an alternative approach to understanding the attenuation, we analysed the Step Frequency GPR (SFGPR) signal in FD. Details about various works with SFGPR can be found in literature (Iizuka et al., 1984; Kong and By, 1995; Langman and Inggs, 2001; Leckebusch, 2011; Noon et al., 1994; Stickley et al., 2000).

In this study, we have adopted cross-hole imaging method using cross-hole radar tomography in which SFGPR data has been analysed separately in TD and FD. While time and amplitude were inverted in TD for velocity and attenuation structures, amplitude at different frequencies was inverted in FD for obtaining frequency domain attenuation. The tomographic imaging method has been applied for imaging the foundation of a dam site with encouraging results. To validate the above observations, cross-hole seismic tomography was also done in the same boreholes.

The organisation of the paper is as follows: Section 2 provides the details of the cross-hole imaging method. Section 3 describes the case study wherein the site of cross-hole-tomography survey, data acquisition and implementation of the imaging method. Section 4 discusses the results of the cross-hole imaging and finally Section 5 gives the conclusion of the study.

## 2. Cross-hole imaging method

Cross-hole radar tomography is an inverse problem in which image of the subsurface target and the medium between a pair of boreholes is reconstructed based on the influence rendered by electrical conductivity and dielectric permittivity of the medium through which the wave propagates (Annan, 2005). For inversion, waves transmitted through the medium between a pair of boreholes are measured at constant intervals throughout the depth of the boreholes over a dense network of ray paths between $N_T$ number of transmitter ($T_x$) locations and $N_R$ number of receiver ($R_x$) locations. This results in collection of $N_T \times N_R$ data set. The entire set of data is then inverted using Simultaneous Iterative Reconstruction Technique (SIRT) to generate a 2D tomographic image called tomogram. The tomogram is interpreted in the light of the geological setting in the study area. Details of SIRT are given in Section 2.3.

Cross-hole radar tomography is a robust method (Clement, 2006) as measurements are reliable for closely spaced boreholes and denser acquisition ray paths. In cross-hole radar tomography, the EM waves travel with different velocities influenced by relative dielectric permittivity ($\varepsilon_r$) and are subjected to attenuation due to conductivity (Hinz and Bradford, 2010) and propagation losses (Reynolds, 2000). While velocity is a time domain factor, the attenuation of signal can be studied in time domain as well as in frequency domain.

### 2.1. Time domain tomography

Travel time and amplitude of the TD signal are commonly used to reconstruct velocity tomogram and attenuation tomograms, as it is relatively easier and quicker to get these values from the measured data. Since velocity and attenuation are related to two different electrical properties (electrical conductivity and dielectric permittivity) of the media (Zhou et al., 2001), it is useful to obtain both the tomograms as they can provide complementary information.

Cross-hole velocity tomography is a technique to obtain distribution of velocity in the medium between a pair of boreholes. Velocity tomography is useful in getting a high-resolution image of the medium. The resolution depends on the contrast in the dielectric permittivity in the medium, size of the target and the separation between the $T_x$ and $R_x$ boreholes. In order to reconstruct the velocity structure, an $N_T \times N_R$ matrix of travel times are obtained before inversion using SIRT (Section 2.3). The resulting velocity image, known as cross-hole radar Velocity Tomogram (VT), is the distribution of wave velocity in the plane separating the boreholes. VT enables identification of anomalous velocity zones lying between the boreholes as well as imaging individual velocity layers.

In attenuation tomography, the amplitude of the signal recorded at the receiver positions throughout the length of the borehole is used for generating attenuation tomogram (Holliger et al., 2001; Zhou and Fullagar, 2001). In situations, where the contrast in dielectric permittivity of the target and the host medium is poor and the medium or target is conductive, the attenuation tomogram holds better information than its velocity counterpart on the property of the medium as the propagation of radar wave amplitude is highly influenced by conductivity (Annan, 2005; Zhou et al., 2001). In order to reconstruct the attenuation structure, $N_T \times N_R$ matrix of amplitudes are obtained and inverted using SIRT (Section 2.3). The resulting attenuation structure in the plane separating the boreholes is called as cross-hole radar Attenuation Tomogram (RAT).

### 2.2. Frequency domain tomography

When radar wave velocity in a medium does not vary significantly, the radar wave attenuation becomes a crucial factor to understand the properties of the medium. Such situations arise when the medium is a complex geological setting, characterised by poor electrical contrasts and high conductivity or attenuation. It is well known that, small fault zones or fractures are normally more conductive compared to the surrounding media and affect the propagation of EM waves (Haeni et al., 2002; Lane et al., 1994; Stolarczyk and Fry, 1990). Therefore, studying the amplitude variations at different frequencies could yield more information on the subsurface medium. This is because, variation in the amplitude with frequency is quite significant (Jha et al., 2003, 2004; Neto and de Medeiros, 2005) even for low to moderate conductive losses in the media. Hence, an attempt was made to study the variation

amplitude in the frequency domain. This led to development of a new technique called Frequency Domain Attenuation Tomography (Jha et al., 2004).

SFGPR transmits a continuous sinusoidal step frequency signal, which is mathematically represented as (Kong and By, 1995)

$$F(t) = Ae^{i2\pi(f+n\Delta f)t} \quad \frac{n-1}{N}T \le t \le \frac{n}{N}T \tag{1}$$

where $A$ is the amplitude of the signal and $n\Delta f$ designates the nth frequency step interval, $\Delta f$, $N$ is the total number of step frequencies and $T$ is the fundamental period of the signal. The SFGPR transmits waveform frequency tones stepped with $\Delta f$, which are highly stable and uniformly spaced across a wide fractional bandwidth. The spectrum of the received signal is expressed as

$$F(f) = S_{dc}(f) + a\ S_R(f)e^{i2\pi ft} \tag{2}$$

where $S_{dc}(f)$ is the spectrum of the direct coupling between the transmitter and receiver and $S_R(f)$ is the spectrum of the received signal and '$a$' is the coefficient. In the case of cross-hole tomography survey, since the transmitter and receiver inside the boreholes are separated by a constant distance, the direct coupling signal becomes insignificant and hence, it can be neglected in Eq. (2). The SFGPR spectrum, $S_R(f)e^{\ i2\pi ft}$, consists of a combination of radar system response and medium response. When the input spectrum and the radar system response are wide-bandwidth and non-dispersive, the received spectrum can be considered the resultant effect of propagation through the in situ property of the medium (Kong and by, 1995). It has been observed that various features are reflected in the tomograms with different representative frequencies based on their size and attenuation properties. Subsequently, the spectrum of the raw data is analysed for variation in amplitude at different frequencies. If inversion of amplitude at single representative frequencies is judiciously made, images with improved resolution can be obtained. Thus, the frequencies whose amplitude-variation is at least 0.2 times the maximum spectrum amplitude recorded are identified. This minimum variation is required to obtain a discernible attenuation structure. The amplitude values corresponding to such frequencies are extracted from the raw spectrum. A matrix ($N_T \times N_R$) of such amplitude values corresponding to each frequency $f$ are thus obtained and were then inverted using SIRT (Section 2.3) resulting in cross-hole Frequency Domain Attenuation Tomogram (FDAT) that depicts the structure of attenuation in the tomographic plane.

Since the spectral response to different types of target is different, FDAT is different from the approach of Cote et al. (1995), who used amplitudes corresponding to mono-frequency signals transmitted at different depths. When the spectral response at different frequencies is segregated and studied, more information on the nature of the target and medium can be deciphered. This is demonstrated in the FDAT approach. Analysing amplitudes at frequencies that are representative of subsurface responses is equivalent to obtaining frequency-filtered amplitude. Frequency domain attenuation at such individual frequencies holds a better chance of resolving the target than attenuation using the TD amplitude.

### 2.3. Inversion of the cross-hole radar tomography data

In inversion, a model of a subsurface area under investigation is estimated in terms of velocity and attenuation, using time and amplitude data sets, $D$, from the area. The initial estimate can be solved by iterative algorithm SIRT, which is straight line ray inversion technique. The SIRT algorithm is a finite series-expansion method (Dines and Lytle, 1979; Gilbert, 1972; Ivansson, 1986; McMechan et al., 1987; Stewart, 1992) based on the Algebraic Reconstruction Technique (ART). Gordon (1974), Censor (1983) and Peterson et al. (1985) give details of ART algorithm. The ART algorithm operates on only one ray path at a time, whereas the SIRT algorithm operates on all the ray paths passing through a given zone simultaneously (McGaughey and Young, 1990). SIRT iteratively updates velocity or attenuation estimates until it matches travel-time data or amplitude, starting from some initial value.

In cross-hole tomography, the cross-hole data $D$, along a ray path $P$, can be expressed as

$$D = \int_P x dr \tag{3}$$

where, $x$ designates the slowness model, d$r$, the increase in the ray path length. The ray path $P$ is the straight line connecting a transmitter point and receiver point. This model ($x$) is then used to reconstruct the velocity and attenuation structures from the acquired data. Such inverse problem is solved by linear functions relating the model and the acquired data and casting the inverse problem as an iterative linear perturbation problem. The slowness $x_j$ assigned to a cell, $j$, for a given ray path ($i$) of travel time or amplitude ($D_i$) is expressed as

$$\delta D_i \approx \sum_j \frac{\partial D_i}{\partial x_j}\delta x_j \tag{4}$$

where $D_i$ represents the data propagating along the $i$th ray, $x_j$ is the modelled value in the $j$th cell.

This equation can be re-written in the form

$$D = [W]x \tag{5}$$

where $D$ is n-component vector of the travel time or amplitude residuals, $x$ is the m-component vector of the perturbation of the subsurface model and $W$ is the matrix of partial derivatives relating $D$ and $x$. The matrix of partial derivatives of vector

$$W = \begin{pmatrix} W_{11} & W_{12}\ldots & W_{1j} \\ W_{21} & \ddots & \vdots \\ W_{31} & & \\ W_{i1} & \cdots & W_{ij} \end{pmatrix}. \tag{6}$$

The vector component $W_{ij}$ of $i$th ray in $j$th cell in the matrix of $W$ is given by $\frac{\partial D_i}{\partial x_j}$.

The inversion model is built by dividing the plane separating the radar transmitter and receiver holes into a mesh of grid cells known as finite elements (Fig. 1). Each element in the mesh is assigned an initial value ($x_0$) for the time or amplitude considered, and the synthetic travel time or amplitude for the portion of each ray path passing through the grid cells is calculated. The initial value is estimated based on the time or amplitude value at the centre of the grid.

Starting from $x_{0,}$ the iterative technique solves for $x$ in Eq. (5) toward improved solutions using the update equation

$$x_{k+1} = x_k + \Delta x_k \tag{7}$$

where $k$ denotes the iteration number and $\Delta x_k$, is the error term.

ART considers each row of $W$ in turn, adjusting each component of $x$, such that each component $\Delta \mathbf{x}_{kj}$ of $\Delta x_k$ is given by

$$\Delta x_{kj} = \frac{D_i - \sum_{a=1}^{b} W_{ia}x_a}{\sum_{a=1}^{b} W_{ia}^2} W_{ij}. \tag{8}$$

SIRT implements the ART update of Eq. (5), but the corrections are saved until an entire iteration (all rows) is completed. The mean correction vector is applied, weighted component-by-component by the number of non-zero elements in the appropriate column of $W$. The

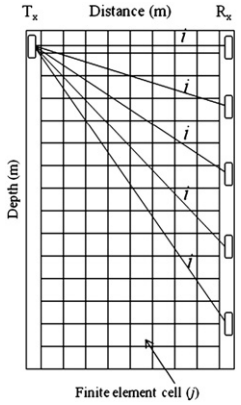


**Fig. 1.** SIRT inversion model uses straight rays and cells between the boreholes in the tomographic plane area (A); propagation paths (denoted "i") through each cell are used in the simultaneous iteration process towards minimising the error between the model and measured values.

SIRT update equation is given by Eq. (9), where the $j$th component of $\Delta x_k$ is given by

$$\Delta x_{kj} = \frac{1}{U_j}\sum_{i=1}^{n}\frac{D_{i-}\sum_{a-1}^{m} W_{ia}x_a}{\sum_{a=1}^{m} W_{ia}^2} W_{ij} \tag{9}$$

where $U_j$ is the number of non-zero components in the column vector $W_{ij}$.

The mesh representing the tomographic plane is divided into $X$ number of cells along the distance between the two boreholes and $Y$ number of cells along the depth of the boreholes, resulting in a mesh of $(X \times Y)$ cells. The total travel time or resultant amplitude for each ray path in the mesh is built up and then compared to the measured travel time or amplitude. The velocities or attenuation assigned to the various elements are then adjusted iteratively until the calculated and measured travel times or amplitudes for the ray path converge within an RMS error limit of 0.001 dB for amplitude and 0.01 ns for time. The iteration stops at this stage and produces the reconstructed image between the boreholes.

In SIRT, the ray paths intersect a number of cells in their path resulting in accurate estimates of the velocity or attenuation for each cell. Since the density of rays in the central portion between the boreholes is high compared to that at the edges, this difference causes SIRT to assign errors to the cells at the edges. Thus, the error in the edges of the model is less constrained compared to the central part and thus, the uncertainty in limiting the error is greater at the edges (Clement and Knoll, 2000). Using the SIRT algorithm smoother and better looking reconstructions are usually obtained at the expense of slower convergence. Corresponding to the time or amplitude input to the SIRT, the velocity or attenuation tomograms are obtained.

## 3. Case study

### 3.1. The site of cross-hole tomography survey

The site of the cross-hole tomography investigation is an RCC dam (schematic plan in Fig. 2), located in the Lesser Himalayan region. The geological setting of the Lesser Himalayas is highly complex and offers challenges to major construction projects. Geologically the site is predominantly characterised by quartzitic phyllite in jointed form with the phyllite exposed at the surface, thinly bedded phyllite, sheared phyllite and phyllitic quartzite. At many places, major joints dipping towards WSW with shearing effects were noticed in the phyllites. Majority of the foliation joints were dipping downstream. Due to intersection of the WSW dipping joints with foliation joints, structural wedges have been formed in the foundation and these wedges have led to uneven foundation surface.

Various geological, geophysical and geotechnical investigations are generally done for deciphering the geological structures and associated rock and rock mass quality at various depths. Depending on strengths and weaknesses in the rock mass, sufficient reinforcement measures, are generally taken to ensure long-term stability of the foundation. Despite all such investigations and design-reinforcements, hidden or dormant geological weak zones might come to the fore posing a challenge for major construction projects, as dormant features are not always detectable. Hence, it is useful to ascertain that the foundation is free of any (dormant) weak zone, given the complex geological setting characterised by shearing in the rock mass. Fig. 3 shows the geological section of the dam site, where some seepage of water was observed during reinforcement measures. Therefore, it was necessary to investigate the foundation. Most feasible location to probe was from the lowest drainage gallery at RL523 m, which was approximately 100 m long and 2.5 m wide, and aligned with the axis of the dam. A 30 m stretch between RD −58 m and −88 m of the gallery was chosen for this cross-hole radar tomography.

The layout of boreholes (Fig. 2 inset) and section-view (Fig. 3) of the four boreholes, between RD −58.4 m to −88.0 m, used in the cross-hole tomography data acquisition are shown in the backdrop of their plan location (Fig. 2) and the geological setting (Fig. 3) respectively. The diameter of each of the boreholes was 74 mm, and the holes were cased with plastic pipes up to the bottom of the borehole. The borehole co-ordinates confirmed the verticality of the boreholes. The location of the four boreholes provided three consecutive pairs of boreholes, with a separation of 10.85 m, 9.25 m and 9.60 m respectively and each plane of separation identified as A, B and C.

### 3.2. Instruments and data acquisition

Fig. 4(A) is the setup of the SFGPR data acquisition system. Kong and By (1995) discuss its operating principle, details of the instrumentation, which uses network analyzer as the transmitter–receiver, performance of this radar, its advantages and disadvantages. A brief description of SFGPR, used in this study, is given in Balasubramaniam et al. (2013). The borehole antennas (Fig. 4B) used in the present data acquisition are passive elements, designed to perform ultra wideband operation. Suitable frequency band is identified through a trial test prior to actual data acquisition. As the cased boreholes were vertical and care was taken in transmitter–receiver positioning in the borehole, possibilities of trivial errors in the tomography data were either avoided or minimised. The uniformity of spacing between the boreholes was also cross-verified with the travel times of radar and seismic waves between transmitter and receiver at different depths of each pair of holes. Data was acquired up to 40 m into the foundation from the drainage gallery floor (RL523 m) in the frequency bandwidth of 250 MHz. The cross-hole radar tomography data was acquired along the entire depth of the planes at 1 m interval.

For cross-hole seismic tomography, a 24-channel digital seismograph was used as the data acquisition unit. The source of seismic signal was an electrical sparker with 4 KV discharge in a short span of time. An electrical signal is sent to trigger the seismograph at the same instant as the electrical discharge thereby eliminating the timing errors associated with triggering. The receiver of the seismic system is a string of rugged, moulded, 12-hydrophones spaced at 1 m. Cross-hole seismic tomography data were acquired at 1 m interval for the same depth by measuring p-wave arrivals. Thus, radar and seismic tomography data sets were generated.

### 3.3. Cross-hole data inversion

The cross-hole data were generally free of noise and this enabled picking of first arrivals and amplitude without resorting to processing (Gheshlaghi and Santamarina, 1998; Tronicke et al., 2000). The radar

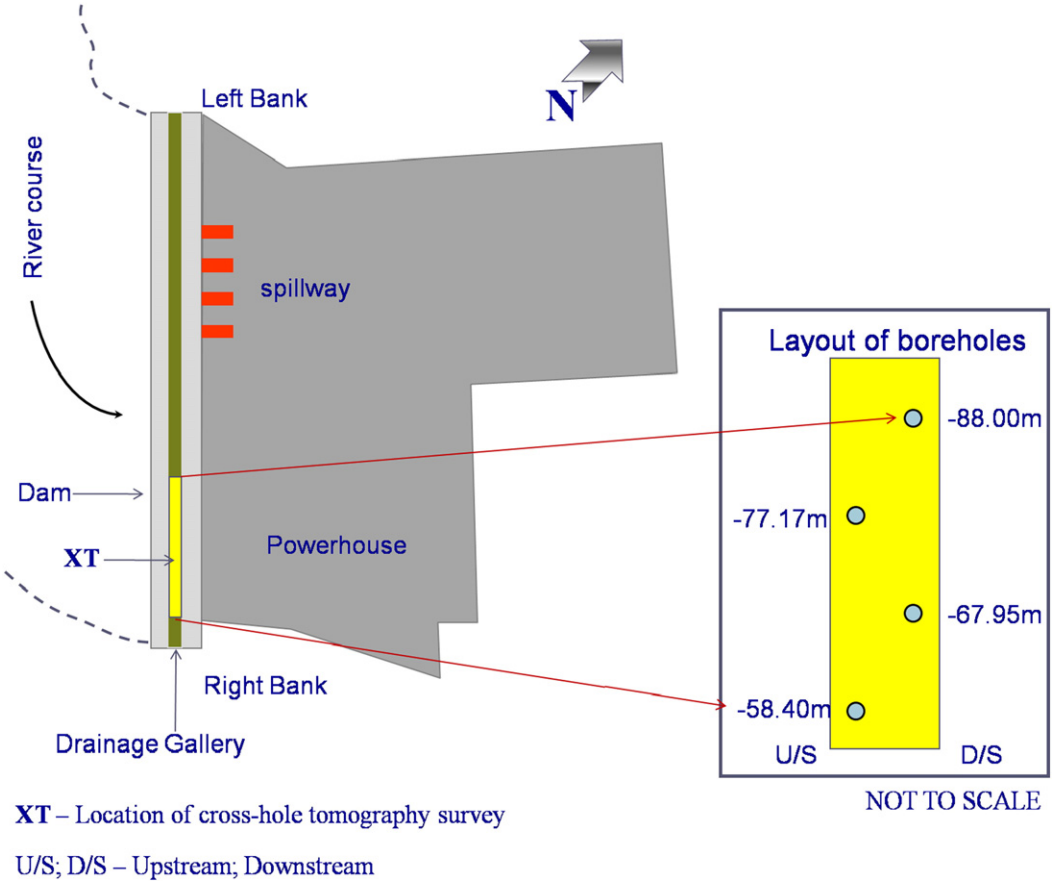


**Fig. 2.** Schematic part plan of the dam, the drainage gallery (zoomed inset) plan layout of the boreholes for the cross-hole tomography survey.

data in time and the frequency domains were analysed and inverted using the cross-hole imaging method (Section 2). For tomographic reconstruction, the plane area separating a borehole-pair was divided into a mesh of 50 cells × 50 cells rendering a cell size of 0.2 m and 0.4 m. The resultant average RMS error of iterations for time and frequency domain data are: VT — 0.00003 ns; RAT — 0.000008 dB; FDAT (100 MHz) — 0.000386 dB; FDAT (200 MHz) — 0.000100 dB. In tandem, cross-hole seismic tomography travel time data was also inverted for p-wave velocity structure (RMS error: 0.005 ms) in the same tomographic planes. The results of inversion of TD and FD parts of the data are discussed in the following section.

## 4. Results and discussion

The final resultant images of the time domain and frequency domain analysis and inversion are discussed in this section, presented in Figs. 5, 6, 7 and 8. For quick identification, each plane separating a pair of boreholes is marked A, B and C, representing each of the planes between, −77.17 to −88.00 m, −67.95 to −77.17 m and −58.40 to −67.95 m respectively. Fig. 5 is a set of three VT showing distribution of radar wave velocity in the foundation. Fig. 6 is a set of three RAT showing the attenuation structure of the radar wave in the foundation. Figs. 7 and 8 show, a set of three FDAT at 100 MHz and 200 MHz respectively, the attenuation structure based on the spectrum-amplitude variation. Finally, Fig. 9 is a comparative presentation of results of the radar frequency-domain data inversion (Fig. 9A) and the seismic arrival time inversion (Fig. 9B).

The VT of plane-C is indicative of a largely homogeneous rock mass with the velocity of radar wave distributed predominantly in the range of 8.5–10.5 cm/ns. The other two tomograms (planes A and B) too exhibit a similar trend of velocity along with a few pockets of higher velocity (11–13 cm/ns) scattered in the entire tomographic plane. These ranges of radar wave velocity are quite indicative of undisturbed rock mass in the foundation. The range of relative permittivity value expected for this range of velocity is 5–9, with occasional excursions up to a maximum of 12.5, which is the characteristic of phyllite (Schön, 1996). The RAT of all the three planes (A, B and C) shows radar attenuation in the range of 5–7 dB/m, with occasional poorly attenuating pockets scattered in the planes A and B. Neither the RATs were showing contrast in attenuation nor did the three VTs showed any correlating velocity zone, indicating that the rockmass might be free from dormant defects.

Subsequently, based on the analysis of amplitude variation at different frequencies attenuation tomograms obtained at two different frequency values 100 MHz (Fig. 7) and 200 MHz (Fig. 8) are compared. The 100 MHz FDAT of the three planes (A, B and C), shows a characteristic attenuation of 6–7.5 dB/m dominating the entire depth range of the planes. There are some isolated and insignificant pockets of lower attenuation (around 5 dB/m) and higher attenuation (8–9 dB/m) in those three planes. The FDAT at 200 MHz too shows a similar attenuation trend as seen for 100 MHz, with three visibly contrasting attenuation zones at different parts of the planes. However, among such zones, there is a notable high attenuation zone (7.5–11 dB/m) in plane-B (Fig. 9A) in the RL range 490–500 m (RD67.95–73 m). This anomalous high attenuation zone obtained at 200 MHz was clearly indicative of a change in the character of rock mass at this depth and is representative of a likely weak zone probably rendered by shearing in the rock mass.

The cross-hole radar tomography results were compared with the cross-hole seismic tomography results obtained in the planes A, B and C. A combined view of the cross-hole radar tomography and cross-hole seismic tomography results is presented in Fig. 9. The three seismic velocity tomograms are 2D reconstruction of p-wave velocity

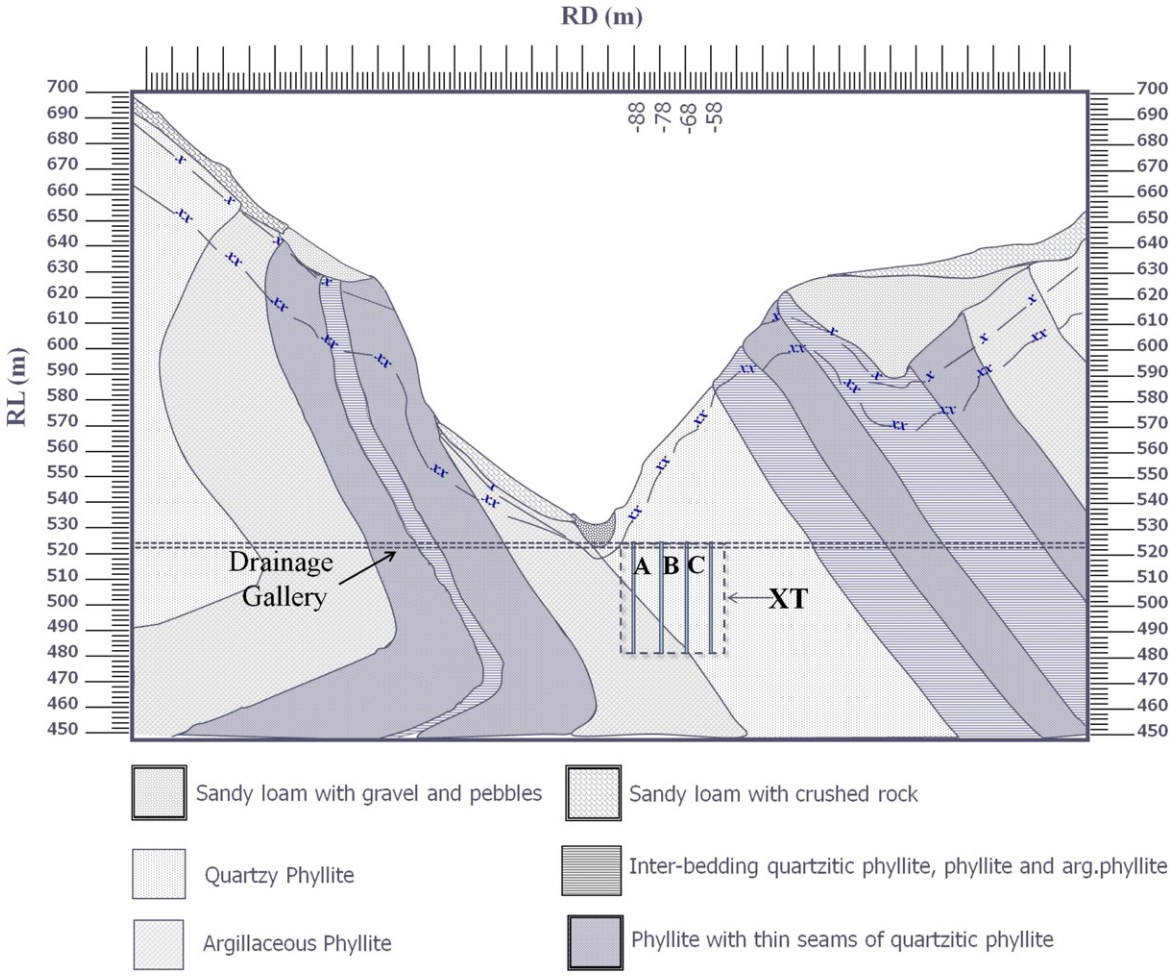


**Fig. 3.** Geological section of the cross-hole tomography site; four boreholes drilled between −58.40 m and −88.00 m; XT is the location of cross-hole tomography survey. A, B and C are the three planes separating three pairs of boreholes.

distribution in the vertical planes. Interestingly, a Low Velocity Zone (LVZ) (2200–3500 m/s) is quite conspicuous in the tomographic plane B (Fig. 9B), which is predominantly characterised by p-wave velocity ranging between >3500 and 5500 m/s. P-wave velocity of this range is normally representative of a good quality rock mass and in this case it is a likely representative of jointed hard phyllite to massive

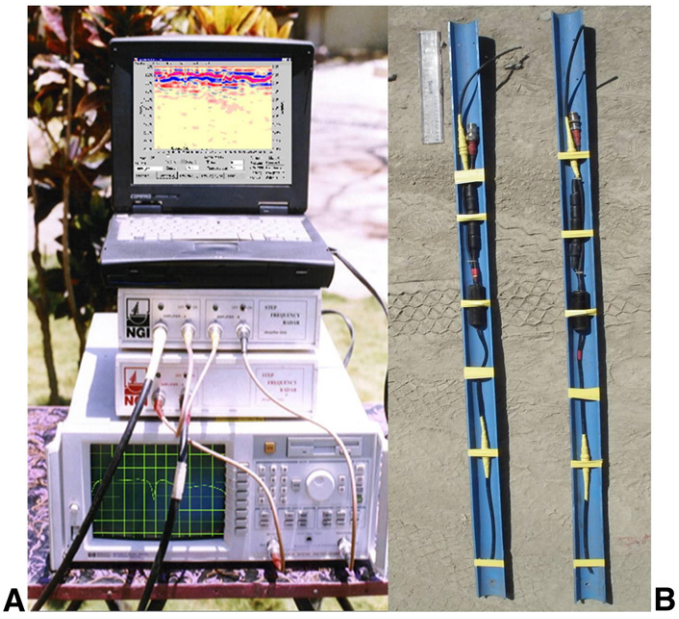


**Fig. 4.** A) Step frequency GPR data acquisition system setup and (B) pair of borehole antennas mounted on cut-plastic pipes.

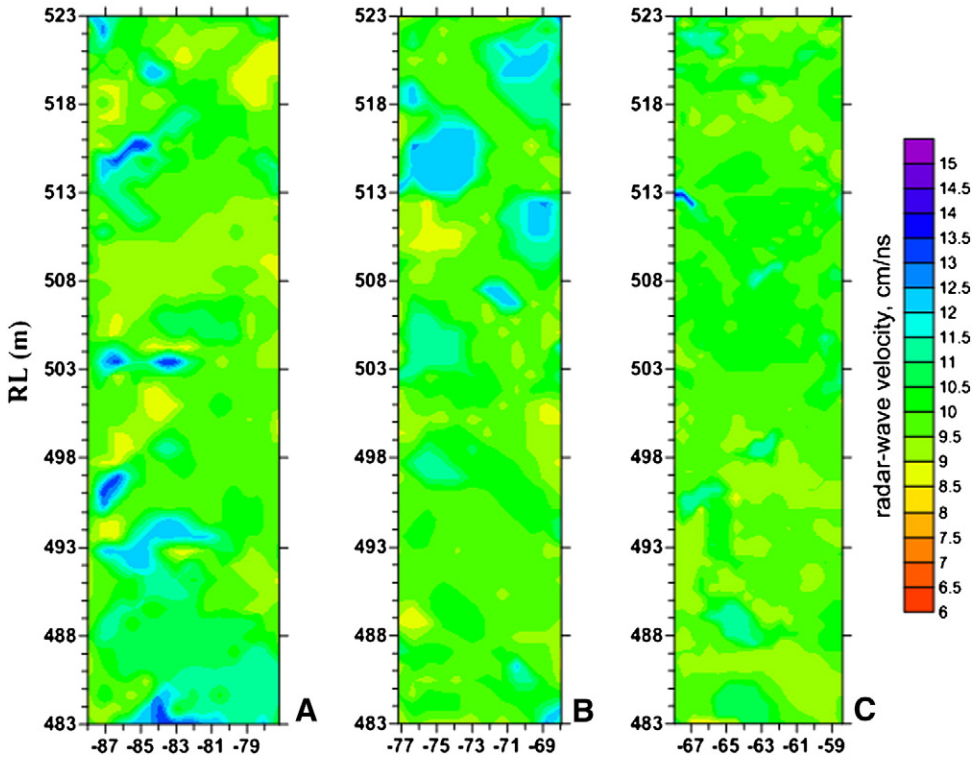


**Fig. 5.** Cross-hole time domain velocity tomograms (VT) showing distribution of radar wave velocity, in the three planes (A, B and C) in the foundation.

phyllite. The velocity range of 2200–3500 m/s is generally observed in situ in weathered rock to highly jointed hard rock. This LVZ is seen at three locations in the depth range of 15–40 m in the host medium whose p-wave velocity is at least 1.5 times higher. Such large variation in the p-wave velocity is quite significant and it clearly indicates that the rock beneath the dam is not uniform in character and there were some zones or patches with lower seismic velocities representing a weak zone with poorer rock quality. Considering the contrast in the seismic velocity, it is likely that the LVZ is due to the weak zone possibly rendered by shearing in the rock mass.

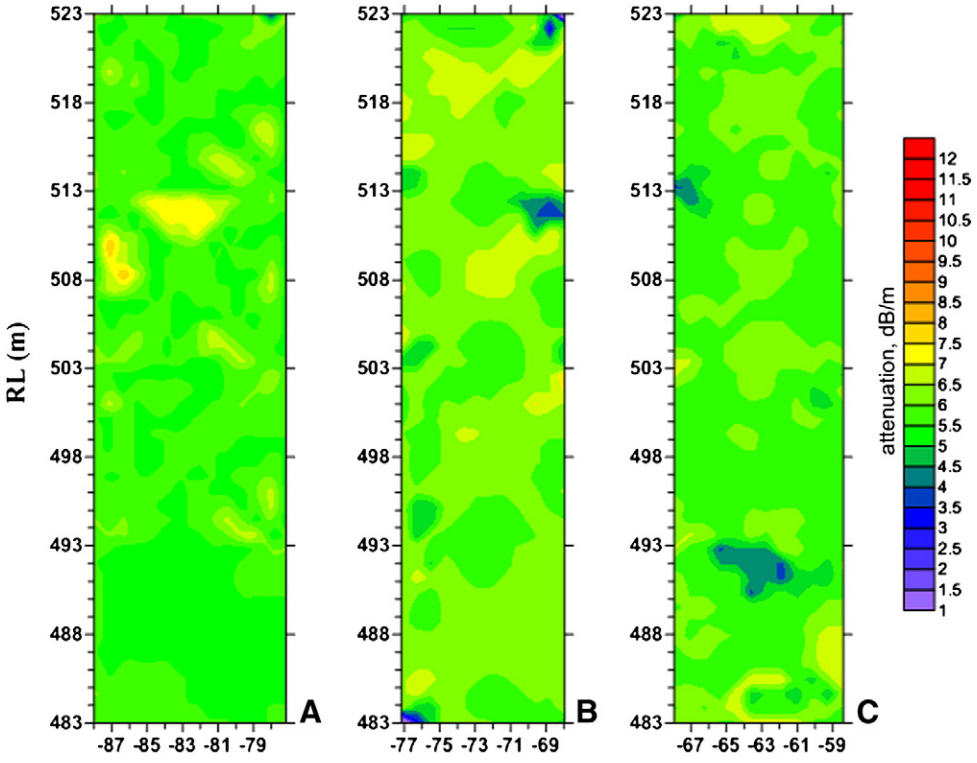


**Fig. 6.** Cross-hole time domain attenuation tomograms (RAT) showing attenuation structure of radar wave, in the three planes (A, B and C) in the foundation.

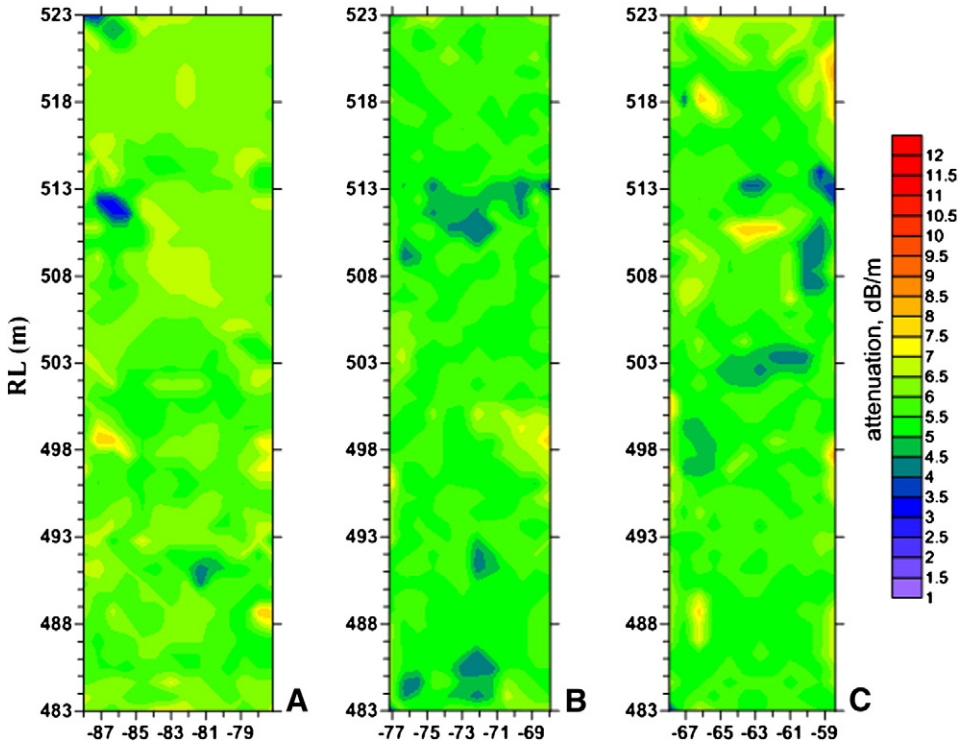


**Fig. 7.** Cross-hole frequency domain tomograms (FDAT) at 100 MHz showing attenuation structure of radar wave in the foundation.

The LVZ of seismic velocity tomogram (Fig. 9B) is a strong indication of a weak zone in the foundation and exists in the same depth range as that of the high attenuation zone (AZ) (7.5–11 dB/m) seen in FDAT at 200 MHz. The size of the LVZ and the AZ correlates well with each other in the plane B (Fig. 9), which confirms beyond doubt that the AZ is truly representative of some weak zone in the rock mass that had remained dormant. The shearing phenomena the rock mass had undergone in the past had possibly rendered such a weak zone and this zone along with a few minor pockets have either remained dormant or undetectable. Since space availability restricted investigation to a 2D plane, understanding the upstream–downstream extension of these weak zones is beyond the scope of the cross-hole imaging. However, in keeping with the geologically mapped shear zones, it is expected that these weak zones in the foundation might follow the trend and dip

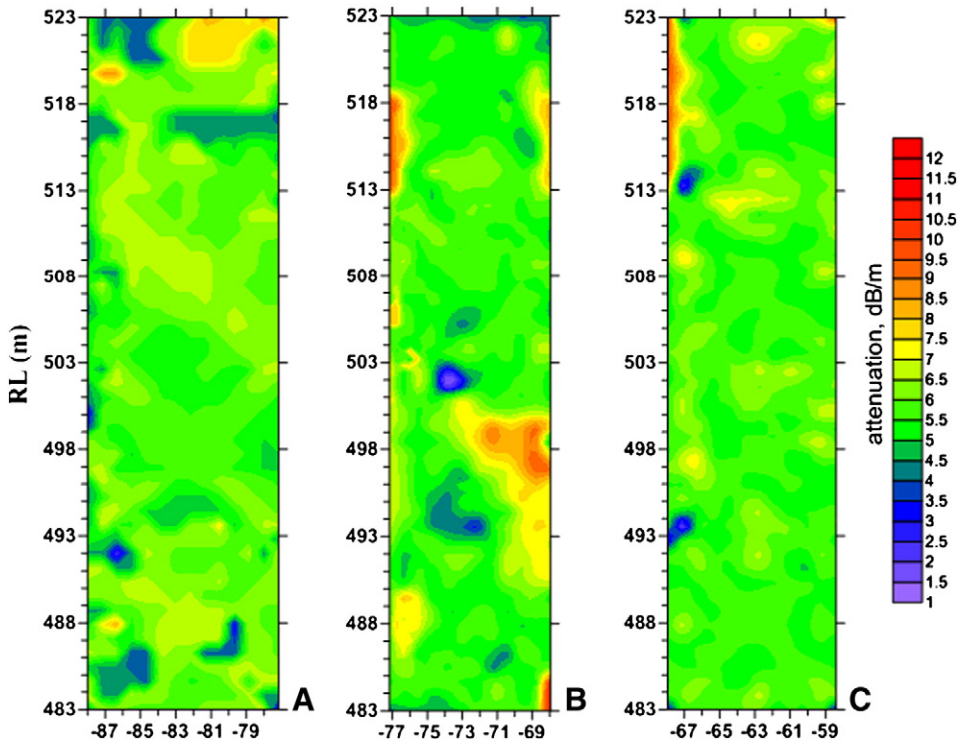


**Fig. 8.** Cross-hole frequency domain tomograms (FDAT) at 200 MHz showing attenuation structure in the foundation. A high attenuation structure (around RL498 m) is seen in plane-B strongly indicating an anomaly in the foundation.

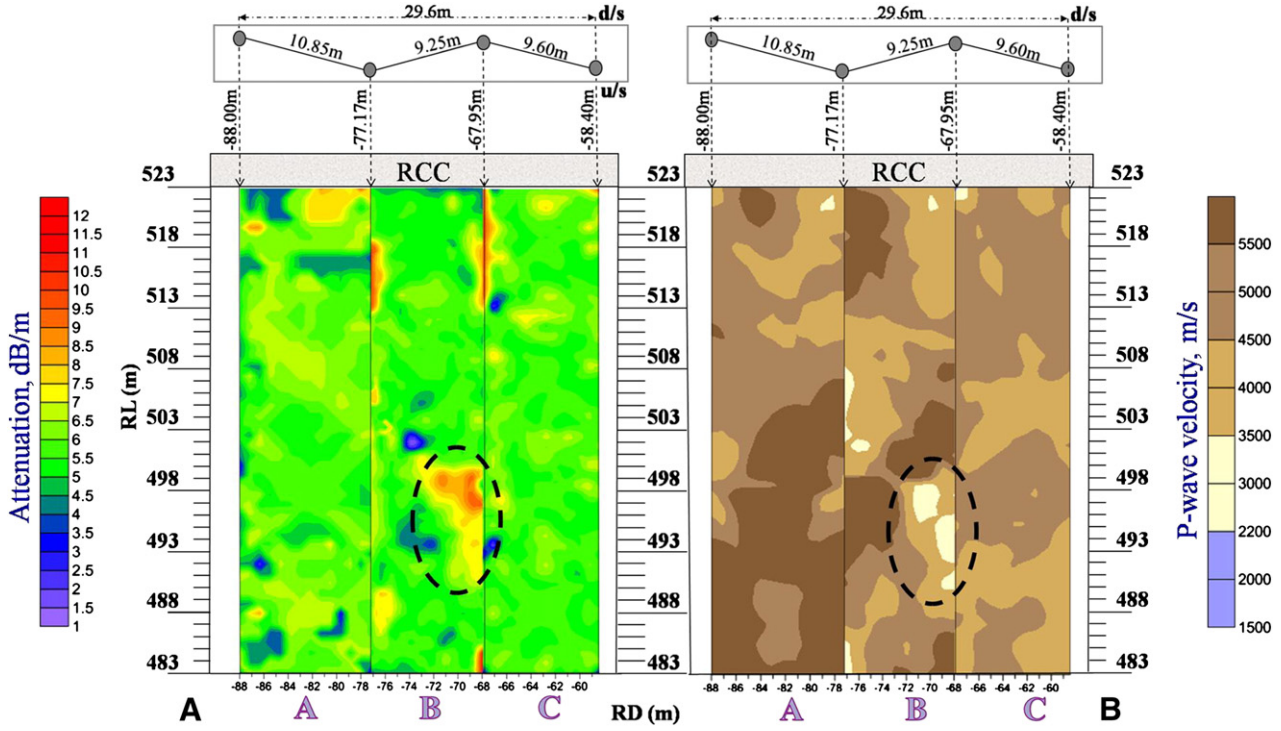


**Fig. 9.** Comparison of the cross-hole radar and seismic tomography results. (A) FDAT tomogram at 200 MHz showing high attenuation zone (7.5–11 dB/m) representing the weak zone (encircled); (B) seismic tomography results showing p-wave low velocity zone (2200–3500 m/s) due to the weak zone (encircled).

in line with the geological setting. Thus, cross-hole radar tomography results were substantiated by the cross-hole seismic tomography results and these identified weak zones were recommended for proper reinforcement.

## 5. Conclusion

The frequency domain approach in analysing the spectrum-amplitude at different single frequencies and the identification of single-effective-frequency were instrumental in locating the high attenuation zone representing a dormant weak zone in the foundation. This has been demonstrated by the frequency domain attenuation tomograms that revealed the weak zone, which otherwise remained elusive in the time domain tomograms. The ability to dissect transmission spectrum in accordance with the media response and target size have proved advantageous in highlighting the dormant weak zone. Higher contrasts in the electrical properties of the rock mass in the foundation could have reflected better on the radar time domain tomograms (velocity or attenuation). The results of cross-hole seismic tomography, which were done for validation purpose, unambiguously complemented FDAT images.

This study instils further interest in the analysis of frequency domain data to understand and take advantage of frequency–rock mass interaction in identifying near surface defects. Tomographic reconstruction based on inversion of spectrum amplitude in the frequency domain appears to be a viable alternative way of the mapping attenuation distribution in a medium and will be useful to obtain an image of the subsurface targets with improved resolution.

## Acknowledgments

The authors are thankful to the authorities of the dam site for providing opportunity and making necessary arrangements at the site for carrying out the cross-hole tomographic experiments. The authors are also thankful to the Director of NIRM for granting permission to publish this work. The authors sincerely thank the Editor-in-chief, guest editors and the anonymous referees for their comments that helped improve the content and quality of the paper.

## References

Angioni, T., Rechtien, R.D., Cardimono, S.J., Luna, R., 2003. Crosshole seismic tomography and borehole logging for engineering site characterization in Sikeston, MO, USA. Tectonophysics 368, 119–137.

Annan, A.P., Cosway, S.W., 1992. Ground penetrating radar survey design. Paper Prepared for the Annual Meeting of SAGEEP, Chicago 1–12.

Annan, A.P., 2005. Ground penetrating radar. In: Butler, D.K. (Ed.), Near Surface Geophysics. Investigations in Geophysics, 13. SEG, p. 732.

Balasubramaniam, V.R., Jha, P.C., Chandrasekhar, E., 2013. Imaging near surface defects using step-frequency ground-penetrating radar. Near Surface Geophysics 11, 19–27. http://dx.doi.org/10.3997/1873-0604.2012044.

Bradford, J.H., 2007. Frequency-dependent attenuation analysis of ground-penetrating radar data. Geophysics 72 (3), 7–16.

Butler, D.K., 2007. Engineering and environmental applications of the potential field methods of geophysics. Symposium on the Application of Geophysics to Engineering and Environmental Problems: , 20 (1), pp. 310–322.

Censor, Y., 1983. Finite series-expansion reconstruction methods. Proceedings of the IEEE 71 (3), 409–419.

Clement, W.P., 2006. Issues during the inversion of crosshole radar data: can we have confidence in the outcome? Journal of Environmental and Engineering Geophysics 11 (4), 269–287.

Clement, W.P., Knoll, M.D., 2000. Tomographic inversion of cross-hole radar data: Confidence in results. Proceedings of the Symposium on the Application of Geophysics to Environmental and Engineering Problems, Arlington, VA, Feb. 20–24 553–562.

Cote, P., Degauque, P., Lagabrielle, R., Levent, N., 1995. Detection of underground cavities with mono-frequency electromagnetic tomography between boreholes in the frequency range 100 MHz to 1 GHz. Geophysical Prospecting 43, 1083–1087.

Dahlin, T., 1996. 2D resistivity surveying for environmental and engineering applications. First Break 14, 275–284.

Davis, J.L., Annan, A.P., 1989. GPR for high resolution mapping of soil and rock stratigraphy. Geophysical Prospecting 375, 531–551. http://dx.doi.org/10.1111/j.1365-2478.1989.tb02221.x.

Deceuster, J., Delgranche, J., Kaufmann, O., 2006. 2D cross-borehole resistivity tomographies below foundations as a tool to design proper remedial actions in covered karst. Journal of Applied Geophysics 60 (1), 68–86.

Deidda, G.P., Ranieri, G., 2005. Seismic tomography imaging of an unstable embankment. Engineering Geology 82, 32–42.

Dines, K., Lytle, J.R., 1979. Computerized geophysical tomography. Proceedings of the IEEE 67, 1065–1073.

Ellefsen, K.J., Mazzella, A.T., Horton, R.J., McKenna, J.R., 2011. Phase and amplitude inversion of crosswell radar data. Geophysics 76 (3), 1–12.

Everett, M.E., 2012. Theoretical developments in electromagnetic induction geophysics with selected applications in the near surface. Surveys in Geophysics 33, 29–63.
Gheshlaghi, F., Santamarina, J.C., 1998. Data pre-processing in cross-hole geotomography. Journal of Environmental and Engineering Geophysics 3 (1), 41–47.
Gilbert, P., 1972. Iterative methods for the reconstruction of three-dimensional objects from projection. Journal of Theoretical Biology 36, 105–117.
Gordon, R., 1974. A tutorial on ART (algebraic reconstruction techniques). IEEE Transactions on Nuclear Science 21 (3), 78–93.
Grandjean, G., Gourry, J.C., Bitri, A., 2000. Evaluation of GPR techniques for civil-engineering applications; study on a test site. Journal of Applied Geophysics 45, 141–156.
Haeni, F.P., Halleux, L., Johnson, C.D., Lane, J.W. Jr, 2002. Detection and mapping of fractures and cavities using borehole radar, in fractured rock 2002, Denver, Colorado, March 13–15. Proc. Werstville, Ohio, National Ground Water Association.
Hinz, E.A., Bradford, J.H., 2010. Ground-penetrating-radar reflection attenuation tomography with an adaptive mesh. Geophysics 75 (4), 251–261. http://dx.doi.org/10.1190/1.346787.
Hinze, W.J., 1990. The role of gravity and magnetic methods in engineering and environmental studies. In: Ward, S.H. (Ed.), Geotechnical and Environmental Geophysics: Soc. Expl. Geophys., I, pp. 75–126.
Holliger, K., Musil, M., Maurer, H.R., 2001. Ray-based amplitude tomography for cross hole georadar data: a numerical assessment. Journal of Applied Geophysics 47, 285–298.
Ivansson, S., 1986. Seismic borehole tomography — theory and computational methods. Proceedings of the IEEE 74 (2), 328–338.
Iizuka, K.A., Freundorfer, P., Wu, K.H., Mori, H., Ogura, H., Nguyen, V.K., 1984. Step frequency radar. Journal of Applied Physics 56, 2572. http://dx.doi.org/10.1063/1.334286.
Jha, P.C., Balasubramaniam, V.R., Gupta, R.N., Sivaram, Y.V., Nelliat, S., 2002. Engineering geophysical investigations for evaluating stability of excavations and foundations in hydroelectric projects. National Sem. on Modern Trends in Geoscientific Techniques, Geotechniques: 2002, India..
Jha, P.C., Balasubramaniam, V.R., Nelliat, S., Gupta, R.N., Sivaram, Y.V., 2003. Evaluating stability of dam foundations by borehole and surface survey using step frequency radar. Proceedings of the International Symposium on Fusion Technology, South Korea, pp. 355–363.
Jha, P.C., Balasubramaniam, V.R., Nelliat, S., Sivaram, Y.V., Gupta, R.N., 2004. Frequency domain attenuation tomography (FDAT) — a new approach in defect mapping using GPR. Proceedings of the 10th International Conf. on Ground Penetrating Radar, June 21–24, 2004, Delft, The Netherlands, 1, pp. 253–256.
Jung, Y., Kim, J., 1999. Application of anisotropic georadar tomography to monitor rock physical property changes. Journal of Environmental and Engineering Geophysics 4 (2), 87–92.
Klotzsche, A., van der Kruk, J., Meles, G.A., Doetsch, J., Maurer, H., Linde, N., 2010. Full-waveform inversion of cross-hole ground-penetrating radar data to characterize a gravel aquifer close to the Thur River, Switzerland. Near Surface Geophysics 8, 635–649.
Kong, F.N., By, T.L., 1995. Performance of a GPR system which uses step frequency signals. Journal of Applied Geophysics 33 (1–3), 15–26.
Lane Jr., J.W., Haeni, F.P., Williams, J.H., 1994. Detection of bedrock fractures and lithologic changes using borehole radar at selected sites. Proceedings of the 5th International Conf. on Ground Penetrating Radar, Kitchener, Ontario, Canada, June 12–16, pp. 577–592.
Langman, A., Inggs, M.R., 2001. Pulse versus stepped frequency continuous wave modulation for ground penetrating radar. Proceedings of International Geoscience and Remote Sensing Symposium, IGARSS '01, IEEE, pp. 1533–1535. http://dx.doi.org/10.1109/IGARSS.2001.976902.
Leckebusch, J., 2011. Comparison of a stepped-frequency continuous wave and a pulsed GPR system. Archaeological Prospection 18, 15–25. http://dx.doi.org/10.1002/arp.396.
Liu, L., Lane, J.W., Quan, Y., 1998. Radar attenuation tomography using the centroid frequency downshift method. Journal of Applied Geophysics 40, 105–116.
McGaughey, W.J., Young, R.P., 1990. Comparison of ART, SIRT, Least-Squares and SVD two-dimensional tomographic inversions of field data. SEG Annual Meeting, September 23–27, San Francisco, California.
McMechan, G.A., Harris, J.M., Anderson, L.M., 1987. Crosshole tomography for strongly variable media with applications to scale model data. Bulletin of the Seismological Society of America 77, 1945–1960.
Neto, P.X., de Medeiros, W.E., 2005. A practical approach to correct attenuation effects in GPR data. Journal of Applied Geophysics 59, 2,140–2,151.
Noon, D.A., Longstaff, I.D., Yelf, R.J., 1994. Advances in the development of SFGPR. Proceedings of the 5th International Conference on Ground Penetrating Radar GPR'94, Kitchener, Ontario, Canada, 117–132, June 12–16, 1994.
Nuzzo, L., Quarta, T., Galati, M.B., Fedi, M., Garofalo, B., 2008. Potential and pitfalls of GPR traveltime tomography for ancient buildings investigation: experiments on a small-scale real and synthetic calcarenitic block. Near Surface Geophysics 2008, 207–219.
Peterson, J.E., Paulsson, B.J.P., McEvilly, T.V., 1985. Applications of algebraic reconstruction techniques to crosshole seismic data. Geophysics 50 (10), 1566–1580.
Pellerin, L., 2002. Applications of electrical and electromagnetic methods for environmental and geotechnical investigations. Surveys in Geophysics 23, 101–132.
Quan, Y., Harris, J.M., 1997. Seismic attenuation tomography using the frequency shift method. Geophysics 62 (3), 895–905.
Reynolds, J.M., 2000. An Introduction to Applied and Environment Geophysics. John Wiley and Sons.
Schön, J.H., 1996. Physical properties of rocks: fundamentals and principles of petrophysics. In: Helbig, K.T. (Ed.), Handbook of Geophysical Exploration. Elsevier, New York, p. 583.
Saito, H., Shima, H., Toshioka, T., 1990. Application of geotomography to rock investigations. Proceedings of the Symposium on the Application of Geophysics to Engineering and Environmental Problems (SAGEEP), pp. 279–293.
Steeples, D.W., 2001. Engineering and environmental geophysics at the millennium. Geophysics 66 (1), 31–35.
Stewart, R.R., 1992. Exploration seismic tomography-fundamentals. In: Domenico, S.N. (Ed.), Course Notes Series, 3. SEG, Tulsa, Oklahoma.
Stickley, G.F., Noon, D.A., Cherniakov, M., Longstaff, I.D., 2000. Gated stepped-frequency ground penetrating radar. Journal of Applied Geophysics 43 (2–4), 259–269.
Stolarczyk, L., Fry, R.C., 1990. Radio imaging method (RIM) or diagnostic imaging of anomalous geologic structures in coal seam waveguides. Transactions of the Society for Mining, Metallurgy, and Exploration 288, 1806–1814.
Tronicke, J., Dietrich, P., Appel, E., 2000. Pre-processing and quality assessment of crosshole georadar data. Proceedings of the 8th International Conference on GPR, Gold Coast, Australia, pp. 23–26.
Valle, S., Zanzi, L., Rocca, F., 1999. Radar tomography for NDT: comparison of techniques. Journal of Applied Geophysics 41 (2–3), 259–269.
Vasco, D.W., Peterson, J.E., Lee, Ha, 1997. GPR velocity tomography in heterogeneous and anisotropic media. Geophysics 62, 1758–1773.
Wadhwa, R.S., Chaudhari, M.S., Saha, A., Mukhopadhyay, R., Ghosh, N., 2009. Deciphering of weak zones using cross-hole seismic tomography. Journal of Indian Geophysical Union 13 (1), 9–16.
Wänstedt, S., Carlsten, S., Tirén, S., 2000. Borehole radar measurements aid structure geological interpretations. Journal of Applied Geophysics 43, 227–237.
Woolery, E.W., 2002. SH-wave seismic reflection images of anomalous foundation conditions at the Mississinewa dam, Indiana. Journal of Environmental and Engineering Geophysics 7 (4), 161–168.
Yule, D.E., Sharp, M.K., Butler, D.K., 1998. Microgravity investigations of foundation. Geophysics 63, 95–103.
Zhou, B., Fullagar, P.K., 2001. Borehole radar conductivity and permittivity tomography. Journal of Applied Geophysics 47, 261–269.
Zhou, C., Liu, L., Lane, J.W., 2001. Nonlinear inversion of borehole-radar tomography data to reconstruct velocity and attenuation distribution in Earth materials. Journal of Applied Geophysics 47, 271–284.